Enhancing Spatial Resolution of PRISMA Hyperspectral Imagery for Lithological and Hydrothermal Alteration Mapping: Case study of Kuh-e-Janja deposit, southeast Iran

Rasoul Lavaei [1], Shojaeddin Niroomand [1*], Amin Beiranvand Pour [2]

[1]School of Geology, College of Science, University of Tehran, Tehran, Iran
[2]Institute of Oceanography and Environment (INOS), Higher Institution Center of Excellence (HICoE) in Marine Science,
University Malaysia Terengganu (UMT), Kuala Nerus 21030, Terengganu, Malaysia
* Corresponding author (rasool.lavaei@ut.ac.ir)

Keywords: PRISMA, Gram-Schmidt, PCA, pan-sharpening, Hydrothermal alteration mapping, Kuh-e-Janja, Iran

Abstract
Hyperspectral remote sensing offers exceptional spectral detail for identifying minerals, but its relatively coarse spatial resolution often limits its use in geological studies. The PRISMA satellite provides 30 m hyperspectral (VNIR–SWIR) data together with a 5 m panchromatic band, creating the possibility of enhancing spatial detail through image fusion. In this study, we applied two established pansharpening methods—Gram–Schmidt (GS) and Principal Component Analysis (PCA)—to PRISMA data from the Kuh-e-Janja porphyry copper deposit in southeastern Iran. Pre-processing included atmospheric correction, removal of water vapor–affected bands, and Minimum Noise Fraction (MNF) transformation. The hyperspectral cube was then fused with the 5 m PAN band to produce sharpened datasets at 5 m ground sampling distance (GSD). Visual inspection showed that both approaches improved spatial clarity, allowing finer recognition of lithological boundaries, alteration halos, drill sites, roads, and structural features that were not easily visible in the native 30 m imagery. Among the two, GS produced sharper edges and maintained more accurate mineralogical color signatures compared with PCA. Quantitative evaluation across 163 bands supported this result, with GS outperforming PCA in all statistical measures, including SAM, RMSE, ERGAS, CC, UIQI, and PSNR. The generation of 5 m hyperspectral datasets demonstrates the value of combining rich spectral information with fine-scale spatial detail. Such fused imagery provides reliable input for advanced classification techniques (e.g., SAM, SVM, OBIA) and offers a practical framework for mineral exploration, particularly in arid and structurally complex terrains where subtle geological variations are critical to detection.

1. Introduction

Porphyry copper deposits (PCDs) are epigenetic, intrusion-related orebodies characterized by large tonnage and relatively low grades, and they are commonly exploited through bulk (mass) mining methods. They represent the world's principal source of Cu and Mo and also provide an important contribution to global Au resources (Sillitoe, 2010). Porphyry mineralization is closely associated with hydrothermal alteration minerals and zones, which serve as important indicators for exploring such mineral deposits (Cannell et al., 2005). The alteration architecture of porphyry systems commonly comprises potassic, phyllic, and propylitic assemblages, and is frequently overlain by a lithocap characterized by residual silica and advanced argillic alteration (Sillitoe, 2010). These alteration halos may extend several kilometers both laterally and vertically, and their extent is strongly controlled by the size and style of mineralization, the composition of ore-forming fluids, the structural framework, the physical properties of the host rocks, and, most importantly, the degree of erosion (Cooke et al., 2014). In particular, multispectral and hyperspectral images allow the recognition of hydrothermal alteration minerals characterized by their unique spectral absorption and emission features in the visible and near-infrared (VNIR), shortwave infrared (SWIR), and thermal infrared (TIR) (Mars and Rowan 2006, Pour et al., 2025). Hyperspectral (HS) remote sensing images have the extraordinary ability to simultaneously capture visual images and spectral details of objects of interest. These images contain multiple narrow spectral bands in the visible near-infrared (VNIR) to shortwave infrared (SWIR) (Ghamisi et al., 2017; Bedini, 2017; Peyghambari and Zhang, 2021). The broad spectral information represented by hyperspectral data enables the differentiation of different alteration minerals (Eismann et al., 2009; Loizzo et al., 2018).

The Italian Space Agency's PRISMA satellite (PRecursore IperSpettrale della Missione Applicativa) (Loizzo et al., 2019), launched in 2019, is the first spaceborne hyperspectral mission with co-registered panchromatic imaging. Its imaging spectrometer records ~239–250 bands between 400–2500 nm (VNIR and SWIR), with <12 nm spectral resolution. PRISMA's hyperspectral sensor operates in push broom mode with a 30 km swath, yielding a ground sampling distance (GSD) of about 30 m. Crucially, PRISMA carries a parallel high-resolution panchromatic (broadband) camera with 5 m GSD, perfectly co-aligned with the hyperspectral field of view (Loizzo et al., 2018; Loizzo et al., 2016). This dual-sensor design provides the spectral sensitivity of hyperspectral imaging along with fine-scale spatial details from the panchromatic band. Such a combination is ideal for geological applications: the hyperspectral bands can discriminate mineralogy, while the PAN band enhances the spatial definition of geological features. However, the raw 30 m hyperspectral data may miss small alteration zones or detailed lithological contacts that are key in porphyry systems. One of the primary limitations of the PRISMA sensor, as is the case with most spaceborne hyperspectral imaging systems, is its relatively coarse spatial resolution. With a ground sampling distance of 30meters, subtle mineralogical heterogeneities and narrow hydrothermal alteration features may be spatially averaged or entirely missed. This limitation in spatial detail significantly constrains the sensor's effectiveness for high-resolution geological mapping and the accurate delineation of complex structural patterns. Pansharpening and image fusion are among the most widely used and effective strategies for improving the spatial resolution of hyperspectral (HS) imagery (Dian et al., 2021; Vivone, 2023; Wang et al., 2021). In HS–PAN pansharpening, the spatial detail contained in a high-resolution, single-band panchromatic (PAN) image is integrated with the hyperspectral data to enhance its geometric quality while preserving spectral information. For this reason, spaceborne HS sensors such as PRISMA are typically designed to acquire a synchronous high-resolution PAN band alongside the HS cube. Pansharpening methods were the first to be applied, relying on the established use of this technique to improve the spatial resolution of MS images (Vivone et al., 2021). However, because of the substantial mismatch between the spectral range of panchromatic (PAN) bands and the broader hyperspectral (HS) spectrum, HS–PAN pansharpening often introduces both

This contribution has been peer-reviewed. The double-blind peer-review was conducted on the basis of the full paper.
https://doi.org/10.5194/isprs-annals-X-4-W8-2025-441-2026

spectral and spatial distortions (Brezini and Deville, 2023; Dian et al., 2018).

In this study, we employ both Gram–Schmidt spectral sharpening (GS) and Principal Component Analysis (PCA) approaches to pansharpen PRISMA hyperspectral imagery over the Kuh e Janja porphyry copper deposit in southeastern Iran. The Gram–Schmidt method orthogonalizes the hyperspectral bands and substitutes the first component with the high resolution PAN data, effectively injecting fine spatial structure into all spectral channels. This technique – and its adaptive variants – is a well established pan sharpening method in the remote sensing literature (Laben and Brower, 2000) . In contrast, the PCA method transforms the correlated hyperspectral bands into uncorrelated principal components, replacing the first component (PC1), which often resembles the PAN image, with the high resolution PAN band before applying the inverse PCA transform. Both methods are well established in the remote sensing literature and have been adapted for hyperspectral fusion (Pohl and Genderen, 1998). By generating a PRISMA hyperspectral dataset at 5 m GSD, we aim to leverage the sensor's rich spectral information for lithological discrimination while attaining the spatial acuity needed to resolve alteration patterns in the deposit. The resulting high resolution hyperspectral imagery should enable more precise mapping of hydrothermal alteration minerals and rock types in the Kuh e Janja deposit, demonstrating the value of integrated spectral–spatial data for mineral exploration.

2. Study Area

The Kuh-e Janja porphyry deposit is located ~60 km southeast of Nehbandan in southeastern Iran, within the northern segment of the Sistan Suture Zone (SSZ). The SSZ is a major tectonic boundary along the Iran–Afghanistan–Pakistan border and represents the Cretaceous suture between the Afghan and Lut blocks, developed during eastward to northeastward subduction of the Sistan Ocean beneath the Afghan block (Camp and Griffis, 1982; Tirrul et al., 1983; Saccani et al., 2010). The deposit lies in the northeastern part of the Zahedan–Nehbandan Magmatic Belt (ZNMB), a northwest-trending Oligocene–Miocene igneous belt extending for ~200 km. Kuh-e Janja forms part of a cluster of porphyry–epithermal systems within the ZNMB, and its intrusive rocks have been dated at 16.5 ± 2.0 Ma (Fig. 1a). The regional geology comprises two main lithologic units: the intrusive hornblende–plagioclase porphyry unit of Early Miocene age, and the volcanic sedimentary pyroclastic Sefidabeh Formation, dated to the Late Cretaceous–Paleocene. The ip unit, hosting the mineralization, is characterized by porphyritic diorite to quartz diorite intrusions and associated basic dykes. A well-developed hornfels aureole occurs within the surrounding flysch sediments adjacent to the porphyry stocks. The Kps unit is composed of alternating volcanic debris-flow deposits, pyroclastic rocks, mudstone, and locally interbedded limestone. The deposit is hosted by deformed flysch sequences of the Sefidabeh forearc basin, which include shale, sandstone, microconglomerate, and limestone. Intrusive activity at Kuh-e Janja occurred in three main stages, consisting of an early mineralized quartz diorite, followed by post-mineral hornblende diorite and later diorite–gabbro dykes trending E–W and NE–SW. The upper part of the stock has been partially eroded and is locally covered by Quaternary alluvial terrace deposits. Extensive hornfels and skarn alteration zones occur along the intrusive contacts, with widths exceeding 400 meters. Mineralization at Kuh-e Janja is typical of porphyry Cu–Mo systems, characterized by stockwork veining and disseminated sulfides (mainly chalcopyrite and molybdenite) hosted in diorite to quartz diorite and hornfelsed flysch. A secondary skarn zone developed in the flysch below the southern margin of the porphyry body (below 200 m elevation). Additionally, polymetallic Au–Ag–Cu–Pb–Zn mineralization occurs in discrete veins (0.1–3 m thick, 100–150 m long) along N075° and N110° orientations within the surrounding flysch (Elyaspour, 2010; Soleymani et al., 2024). Hydrothermal alteration is well zoned. Early potassic alteration is dominant within the porphyry stocks, marked by K feldspar, shreddy biotite, and anhydrite, replacing magmatic biotite and hornblende. This is overprinted by sericitic alteration, with sericite replacing plagioclase. Argillic alteration is localized along fractures due to oxidation of sulfides, while propylitic alteration affects the outer flysch, identified by epidote, chlorite, pyrite, and calcite assemblages. Supergene oxidation has strongly overprinted both the porphyry and polymetallic zones. Chalcopyrite is commonly replaced by chalcocite and covellite, and secondary minerals such as malachite, azurite, cerussite, and iron oxides are present. This oxidation has led to a vertical zonation typical of mature porphyry systems (Fig 1b) (Elyaspour, 2010; Soleymani et al., 2024).

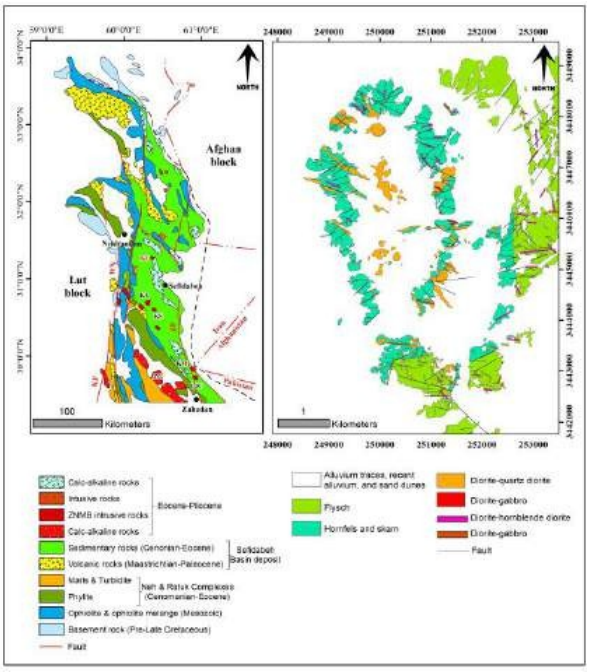

Figure 1. (a) The study area's position in the northern region of the SSZ geological map, along with the simplified outcrop pattern of the Zahedan-Nehbandan magmatic belt (Boomeri et al., 2020; Camp and Griffis, 1982; Tirrul et al., 1983), (b) Simplified geological map of Kuh-e-Janja Porphyry Cu-Au district (modified from Parsolang, 2017).

3. Materials and Methods

3.1 Remote sensing data used

PRISMA acquires hyperspectral imagery in the VNIR–SWIR range using 239 spectral bands, comprising 66 bands in the VNIR and 173 bands in the SWIR. The sensor provides a spectral resolution of ~10 nm and a spatial resolution of 30 m. The sensor provides a scene coverage of 30 km × 30 km. Additionally, panchromatic images are available with a higher spatial resolution of 5 meters (Loizzo et al., 2018). For the present investigation, a Level 2D PRISMA dataset (PRS_L2D_STD_20220314065031_20220314065035_0001

), acquired on 14 March 2022 and covering the Kuh-e-Janja area, was downloaded from the ASI eoPortal (https://prisma.asi.it). The cloud coverage in this dataset was recorded at 1.04%.

3.2 Methodology

Figure 2 shows a schematic diagram of the methodology used in this study. Pre-processing of PRISMA hyperspectral data is essential for accurate surface reflectance and effective analysis. Key steps include removing bad bands affected by water vapor absorption (specifically 913–979 nm, 1078–1185 nm, 1317–1491 nm, and 1775–2044 nm) and correcting spectral distortions like the spectral smile, which shifts central wavelengths across the image (Ceamanos and Doute, 2010). Minimum Noise Fraction (MNF) transformation is applied to reduce image noise, address the smile effect, and determine data dimensionality (Boardman et al., 1995; Green et al., 1988). Subsequently, VNIR and SWIR bands are merged. Finally, atmospheric correction is conducted using the IARR (Internal Average Relative Reflectance) method.

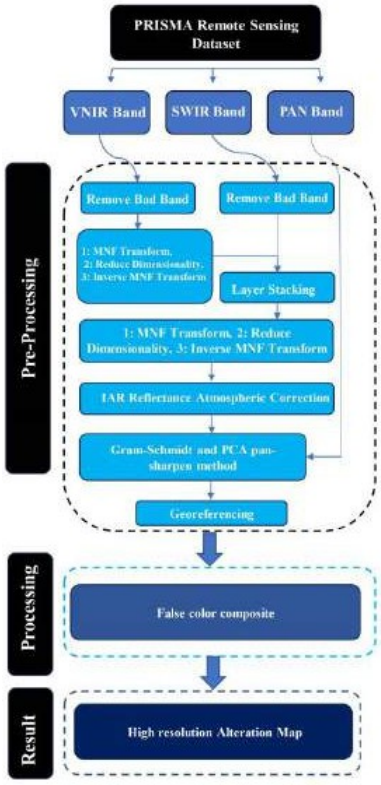

Figure 2. The methodological flowchart utilized in this study.

3.3 Gram-Schmidt (GS) Fusion Method

The Gram-Schmidt (GS) pan-sharpening method stands as a well-established approach for improving the spatial detail of multispectral imagery while preserving its spectral characteristics (Laben and Brower, 2000). This technique merges high-resolution panchromatic (PAN) imagery with lower-resolution multispectral data, optimizing image clarity and minimizing chromatic distortion. The process begins by simulating a PAN band through the averaging of the multispectral bands, which is then used in a forward Gram-Schmidt transformation. The actual high-resolution PAN band is substituted for the first band in the transformation sequence. Subsequently, an inverse transformation is applied to generate pan-sharpened multispectral bands. The method ensures both spectral and spatial fidelity and has been shown to outperform other pan-sharpening techniques.

3.4 Principal Component Analysis (PCA)

PCA is a simple and widely used image fusion technique that transforms correlated multispectral (MS) bands into a set of uncorrelated components (PC1, PC2, …, PCn). The first principal component (PC1), which often resembles the panchromatic (PAN) image, is replaced with the high-resolution PAN band, and the inverse PCA transform is applied to reconstruct the fused image. Similar to the IHS approach, PCA effectively injects spatial details from the PAN band, but it often causes spectral distortion as the dominant spatial information may overwhelm the original spectral characteristics. This issue is sensitive to the selected area and the differences between PC1 and the PAN image; however, adjusting the PAN grey values to match PC1 before replacement can significantly reduce color distortion (Pohl and Genderen, 1998).

In the present study, both the GS and PCA approaches were applied using PRISMA's 5 m resolution panchromatic (PAN) band to enhance the spatial resolution of the 30 m VNIR and SWIR hyperspectral bands. These fusion techniques increased the spatial detail of the hyperspectral data to 5 m while aiming to preserve their original spectral characteristics. Following the fusion process, the resulting images were georeferenced using ground control points (GCPs) to improve positional accuracy, which is essential for generating reliable geological maps and for the precise delineation of alteration and lithological features.

3.5 False Color Composites (FCC)

Adding color to images enhances visual perception and deeper conceptual understanding of the content (Pour et al., 2018). It involves the fusion of three monochromatic spectral bands to generate a composite image that effectively represents surface characteristics (Jun et al., 2008). Typically, digital images use the primary colors red, green, and blue (RGB), each corresponding to specific segments of the electromagnetic spectrum (Di Tommaso et al., 2007). Individually, these bands appear in black and white, but their integration yields a color image that reflects the combined spectral properties. In multispectral imaging, RGB combinations are used to visualize mineral indices, with each mineral displaying unique color signatures based on peak reflectance values (Crosta and Moore, 1989; Hajibapir et al., 2014). By understanding the spectral behavior of surface materials across various wavelengths, appropriate bands can be selected and combined to enhance lithological differentiation and improve diagnostic interpretation of remote sensing data.

3.6 Statistical and Visual Evaluation Methods

Qualitative evaluation, through visual interpretation, involves the observer subjectively assessing the fusion result based on overall and local effects perceived visually. Due to its quick and straightforward benefits, this method has become essential in determining the quality of remote sensing fusion images. In addition to qualitative (visual) evaluation, a quantitative assessment was carried out to objectively evaluate the performance of the fusion methods. For this purpose, six commonly used statistical indices were applied: Spectral Angle Mapper (SAM) for evaluating spectral distortion (Yuhas et al., 1992) , ERGAS as a global indicator of synthesis error (Wald et

al., 1997), Mean RMSE to measure radiometric differences (Zoran., 2009), Mean CC to assess correlation with the reference data (Sarp., 2014), Mean UIQI to quantify overall image quality, and Mean PSNR to evaluate the signal to noise ratio (Zoran., 2009). Together, these metrics provided a comprehensive framework for assessing both spectral fidelity and spatial enhancement of the fused PRISMA imagery.

4. RESULTS & DISCUSSION

Figure 3 demonstrates the improvement in spatial resolution for PRISMA hyperspectral images, from an original 30-meter scale to a refined 5-meter scale. Panel (a) shows the false-color composite (RGB = 87/123/140) at 30 m, selected to emphasize diagnostic absorption–reflection wavelengths for hydrothermal minerals. In this composite, pink to dark-pink hues highlight muscovite–illite (phyllic alteration), light-pink to orange hues depict alunite–kaolinite (argillic alteration), dark-green to bluish-green tones correspond to chlorite– epidote–silica (propylitic alteration and hornfels units), and light-green to yellowish-green hues represent chlorite–epidote– calcite (propylitic alteration and skarn units). Figure(b) presents the co-registered panchromatic band (5 m). Figures (c) and (d) display the fused hyperspectral products at 5 m obtained by the GS and PCA methods, respectively. Together, these panels document the transition from the native 30 m HSI to sharpened 5 m imagery while retaining mineralogical contrast in the composite. Figure 4 compares spatial detail between the original 30 m image (a) and the 5 m fused images produced by GS (b) and PCA (c), with subsets (d–f) provided for direct, local-scale assessment. The native 30 m PRISMA image lacks the spatial acuity needed for deposit-scale interpretation, limiting the ability to discriminate rock units, alteration halos, edges, linear structures, drill collar locations, and roads. In contrast, the 5 m products reveal these features more clearly, with GS offering crisper edges and better preservation of the composite's colorimetric mineral signatures.

In geologically complex terrains like southeastern Iran, lithological units and alteration zones can vary significantly over short distances. Higher spatial resolution helps in distinguishing between similar but distinct units and also the separation of phyllic and argillic alteration zones. This reduces the 'mixed pixel' problem commonly seen in low-resolution hyperspectral data and leads to more accurate lithological classifications and alteration zones.

The quantitative assessment of the pansharpened PRISMA data using the Gram–Schmidt (GS) and Principal Component Analysis (PCA) algorithms highlights distinct differences in performance between the two approaches (Table 1).

Metric	GS	PCA
SAM (deg)	0.490137309	0.590684712
ERGAS	0.714941114	0.743777522
Mean RMSE	0.041268335	0.042734757
Mean CC	0.881511223	0.874356382
Mean UIQI	0.880387202	0.87309524
Mean PSNR	31.43465188	31.15774441

Table 1. Quantitative evaluation of GS and PCA pansharpening methods applied to PRISMA hyperspectral data

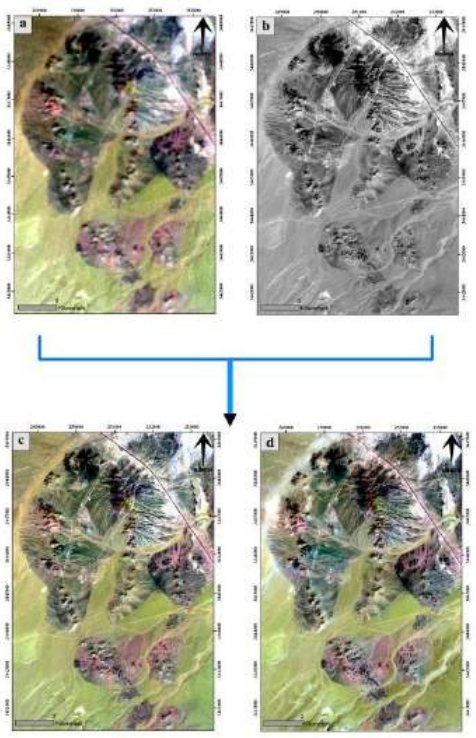

Figure 3. Conversion of PRISMA imagery from 30 m to 5 m spatial resolution using pansharpening algorithms. (a) The original PRISMA image at 30 m resolution; (b) The panchromatic band at 5 m resolution; (c) The fused PRISMA image at 5 m resolution via the GS method; and (d) The fused image at 5 m resolution using the PCA method.

Across all evaluation metrics, the GS method consistently outperformed PCA, albeit with varying degrees of improvement. First, the Spectral Angle Mapper (SAM) values demonstrate that GS is more effective in preserving the spectral integrity of hyperspectral signatures (0.49° for GS vs. 0.59° for PCA). This difference, though seemingly small, is critical in geological applications where the accurate retention of subtle spectral features directly influences the detection of alteration minerals and lithological boundaries. Similarly, the ERGAS and RMSE values confirm the superior accuracy of GS. Both indicators show lower error magnitudes for GS (ERGAS = 0.71; RMSE = 0.041) compared to PCA (ERGAS = 0.74; RMSE = 0.043). These results indicate that GS produces fused images that are not only spectrally reliable but also closer in radiometric fidelity to the original hyperspectral data. The Correlation Coefficient (CC) and Universal Image Quality Index (UIQI) provide further evidence of the robustness of GS. Higher values for GS (CC = 0.88; UIQI = 0.88) compared to PCA (CC = 0.87; UIQI = 0.87) suggest that GS preserves structural and spatial information more effectively, ensuring a better match with the reference hyperspectral cube. Overall, the comparative analysis demonstrates that the GS method provides a more balanced integration of spatial enhancement and spectral fidelity than PCA. While PCA offers computational simplicity and efficiency, it introduces greater distortion to spectral information, making it less suitable for applications requiring high spectral precision. For mineral mapping and hydrothermal alteration studies using PRISMA data, GS emerges as the more reliable technique, particularly due to its superior preservation of diagnostic spectral features.

This contribution has been peer-reviewed. The double-blind peer-review was conducted on the basis of the full paper.
https://doi.org/10.5194/isprs-annals-X-4-W8-2025-441-2026 | © Author(s) 2026. CC BY 4.0 License.

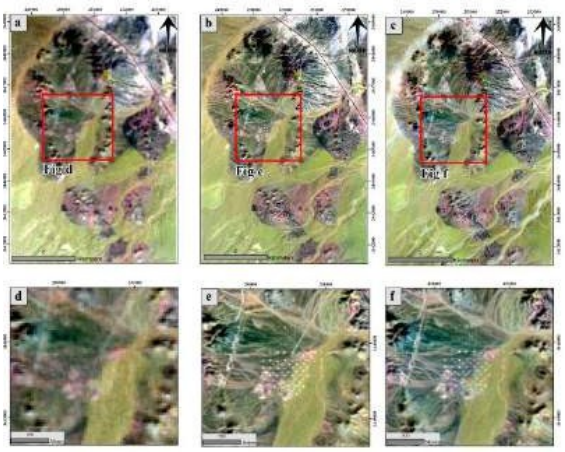

Figure 4. (a) Original PRISMA image with 30 m spatial resolution; (b) Fused PRISMA image at 5 m resolution via the Gram-Schmidt (GS) method.; (c) Fused PRISMA image at 5 m resolution using the PCA method; (d) Subset of the original image highlighting spatial details; (e) Subset of the GS-fused image showing enhanced spatial detail; and (f) Subset of the PCA-fused image showing enhanced spatial detail.

5. Conclusions

This research enhanced the spatial resolution of PRISMA hyperspectral imagery from 30 meters to 5 meters for the Kuh-e-Janja porphyry copper deposit in southeastern Iran by applying two pansharpening methods: Gram-Schmidt (GS) and Principal Component Analysis (PCA). The fused 5 m imagery not only preserved the spectral characteristics associated with alteration minerals but also revealed spatial details—including lithological boundaries, veins, roads, drill-hole locations, and structural features—with significantly improved clarity. Such enhancement is essential for local-scale analysis and geological interpretation in complex terrains. Quantitative evaluation across all 163 bands demonstrated that GS consistently outperformed PCA in every statistical metric. Within the framework of the present dataset and methodology, GS thus emerges as the preferred approach for enhancing the spatial resolution of PRISMA hyperspectral cubes. By achieving an optimal balance between spatial detail and spectral fidelity, the GS method provides a more reliable input for advanced classification algorithms (e.g., SAM, SVM, OBIA), particularly in arid and structurally complex regions such as southeastern Iran, where lithological variations and hydrothermal alteration occur over short distances. By leveraging techniques like Gram-Schmidt pan-sharpening, geoscientists can unlock the full potential of hyperspectral datasets for mineral exploration and geological mapping.

Acknowledgements

The data in this study derive from the lead author's master's thesis, supervised by Shojaeddin Niroomand at the University of Tehran. We extend our heartfelt appreciation to the Iran Minerals Production and Supply Company for providing site access, exploration data, and core logs. We are also grateful to the University of Tehran for furnishing the equipment required to prepare this article, and to the University Malaysia Terengganu (UMT) for supplying the facilities needed for manuscript editing.

References

Bedini, E., 2017: The use of hyperspectral remote sensing for mineral exploration: A review. Journal of Hyperspectral Remote Sensing, 7(4), pp.189-211.

Brezini, S.E., Deville, Y., 2023: Hyperspectral and Multispectral Image Fusion with Automated Extraction of Image-Based Endmember Bundles and Sparsity-Based Unmixing to Deal with Spectral Variability. Sensors. https://doi.org/10.3390/ s23042341.

Boomeri, M., Moradi, R., Stein, H. and Bagheri, S., 2019: Geology, Re-Os age, S and O isotopic composition of the Lar porphyry Cu-Mo deposit, southeast Iran. Ore Geology Reviews, 104, pp.477-494. https://doi.org/10.1016/j.oregeorev.2018.11.018.

Boardman, J.W., Kruse, F.A. and Green, R.O., 1995, January: Mapping target signatures via partial unmixing of AVIRIS data. In Summaries of the fifth annual JPL airborne earth science workshop. Volume 1: AVIRIS workshop.

Camp, V.E. and Griffis, R.J., 1982: Character, genesis, and tectonic setting of igneous rocks in the Sistan suture zone, eastern Iran. Lithos, 15(3), pp.221-239. https://doi.org/10.1016/0024-4937(82)90014-7.

Cannell, J., Cooke, D.R., Walshe, J.L. and Stein, H., 2005: Geology, mineralization, alteration, and structural evolution of the El Teniente porphyry Cu-Mo deposit. Economic Geology, 100(5), pp.979-1003. https://doi.org/10.2113/gsecongeo.100.5.979.

Ceamanos, X. and Douté, S., 2010: Spectral smile correction of CRISM/MRO hyperspectral images. IEEE Transactions on Geoscience and Remote Sensing, 48(11), pp.3951-3959. https://doi.org/10.1109/TGRS.2010.2064326.

Cooke, D. R., Hollings, P., Wilkinson, J. J., Tosdal, R. M., Turekian, H. D. H. K., 2014: 13.14—Geochemistry of porphyry deposits. Treatise on geochemistry, 13, 357-381.

Crosta, A.P., 1989: Enhancement of Landsat Thematic Mapper imagery for residual soil mapping in SW Minas Gerais State, Brazil, a prospecting case history in greenstone belt terrain. In Proceedings of the 7^< th> ERIM Thematic Conference on Remote Sensing for Exploration Geology, 1989.

Di Tommaso, I. and Rubinstein, N., 2007: Hydrothermal alteration mapping using ASTER data in the Infiernillo porphyry deposit, Argentina. Ore Geology Reviews, 32(1-2), pp.275-290. https://doi.org/10.1016/j.oregeorev.2006.05.004.

Dian, R., Li, S., Sun, B., Guo, A., 2021: Recent advances and new guidelines on hyperspectral and multispectral image fusion. Information Fusion 69, 40–51. https://doi.org/10.1016/j.inffus.2020.11.001.

Dian, R., Li, S., Guo, A., Fang, L., 2018: Deep Hyperspectral Image Sharpening. IEEE Trans Neural Netw Learn Syst 29, 5345–5355. https://doi.org/10.1109/ TNNLS.2018.2798162.

Eismann, M.T., Stocker, A.D. and Nasrabadi, N.M., 2009: Automated hyperspectral cueing for civilian search and rescue. Proceedings of the IEEE, 97(6), pp.1031-1055. https://doi.org/10.1109/JPROC.2009.2013561.

Elyaspour, N., 2010: Economic geology and ore mineralization in Sefidabeh area (Kuh-e Janja), east of Iran: Ms. thesis, Zahedan, University of Sistan va Baluchestan, 282 p.

Ghamisi, P., Plaza, J., Chen, Y., Li, J. and Plaza, A.J., 2017: Advanced spectral classifiers for hyperspectral images: A review. IEEE Geoscience and Remote Sensing Magazine, 5(1), pp.8-32. https://doi.org/10.1109/MGRS.2016.2616418.

Green, A.A., Berman, M., Switzer, P. and Craig, M.D., 1988: A transformation for ordering multispectral data in terms of image quality with implications for noise removal. IEEE Transactions on Geoscience and Remote Sensing, 26(1), pp.65-74.

Hajibapir, G., Lotfi, M., Zarifi, A.Z. and Nezafati, N., 2014: Application of different image processing techniques on ASTER and ETM+ images for exploration of hydrothermal alteration associated with copper mineralizations mapping Kehdolan Area (EASTERn Azarbaijan Province-Iran). Open Journal of Geology, 4(11), pp.582-597. https://doi.org/10.4236/ojg.2014.411043.

Jun, L., 2008: Research on False Color Image and Enhancement Methods Based on Ratio Images. The International Archives of the Photogrammetry. Remote Sensing and Spatial Information Sciences, 37, pp.1151-1154.

Laben, C. A., Brower, B. V., 2000: U.S. Patent No. 6,011,875. Washington, DC: U.S. Patent and Trademark Office.

Loizzo, R., Daraio, M., Guarini, R., Longo, F., Lorusso, R., Dini, L., Lopinto, E., 2019, July: Prisma mission status and perspective. In IGARSS 2019-2019 IEEE International Geoscience and Remote Sensing Symposium (pp. 4503-4506). IEEE. https://doi.org/10.1109/IGARSS.2019.8899272.

Loizzo, R., Guarini, R., Longo, F., Scopa, T., Formaro, R., Facchinetti, C., Varacalli, G., 2018, July: PRISMA: The Italian hyperspectral mission. In IGARSS 2018-2018 IEEE international geoscience and remote sensing symposium (pp. 175-178). IEEE. https://doi.org/10.1109/IGARSS.2018.8518512.

Loizzo, R., Ananasso, C., Guarini, R., Lopinto, E., Candela, L., Pisani, A. R., 2016 May: The Prisma hyperspectral mission. In Proceedings of the Living Planet Symposium, ague, Czech Republic (pp. 9–13).

Parsolang, 2017: 1:10000 Geological Map of Geology map of the Janja Cu-Au-Mo deposit: Tehran, Iran Mineral Processing and Processing Company (IMPASCO).

Peyghambari, S. and Zhang, Y., 2021: Hyperspectral remote sensing in lithological mapping, mineral exploration, and environmental geology: an updated review. Journal of Applied Remote Sensing, 15(3), pp.031501-031501. https://doi.org/10.1117/1.JRS.15.031501.

Pohl, C., Van Genderen, J.L., 1998: Multisensor image fusion in remote sensing: concepts, methods and applications. Int. J. Rem. Sens. 19, 823–854.

Pour, A. B., Niroomand, S., Lavaei, R., Mirzaee, S., Habashi, J., & Moghadam, H. J., 2025: 19 Mineral Remote Identification Sensing Data Using. Remote Sensing for Geophysicists, 281.

Pour, A.B., Hashim, M., Park, Y. and Hong, J.K., 2018: Mapping alteration mineral zones and lithological units in Antarctic regions using spectral bands of ASTER remote sensing data. Geocarto International, 33(12), pp.1281-1306. https://doi.org/10.1080/10106049.2017.1347207.

Rowan, L.C., Schmidt, R.G. and Mars, J.C., 2006: Distribution of hydrothermally altered rocks in the Reko Diq, Pakistan mineralized area, based on spectral analysis of ASTER data. Remote sensing of Environment, 104(1), pp.74-87. https://doi.org/10.1016/j.rse.2006.05.014.

Saccani, E., Delavari, M., Beccaluva, L. and Amini, S., 2010: Petrological and geochemical constraints on the origin of the Nehbandan ophiolitic complex (eastern Iran): Implications for the evolution of the Sistan Ocean. Lithos, 117(1-4), pp.209-228. https://doi.org/10.1016/j.lithos.2010.02.016.

Sarp, G., 2014: Spectral and spatial quality analysis of pan-sharpening algorithms: A case study in Istanbul. European Journal of Remote Sensing, 47(1), pp.19-28.

Sillitoe, R.H., 2010: Porphyry copper systems. Economic geology, 105(1), pp.3-41. https://doi.org/10.2113/gsecongeo.105.1.3.

Soleymani, M., Monecke, T., James Reynolds, T. and Niroomand, S., 2024: Mineral paragenesis of early biotite veins at the Kuh-e Janja Cu-Au porphyry deposit, southeastern Iran: Importance of microtextural observations in studies constraining the relative timing of hypogene Cu mineralization. Economic Geology, 119(5), pp.1199-1208. https://doi.org/10.5382/econgeo.5082.

Tirrul, R., Bell, I.R., Griffis, R.J. and Camp, V.E., 1983: The Sistan suture zone of eastern Iran. Geological Society of America Bulletin, 94(1), pp.134-150.

Vivone, G., 2023: Multispectral and hyperspectral image fusion in remote sensing: A survey. Information Fusion 89, 405–417. https://doi.org/10.1016/j. inffus.2022.08.032.

Vivone, G., Mura, M.D., Garzelli, A., Restaino, R., Scarpa, G., Ulfarsson, M.O., Alparone, L., Chanussot, J., 2021: A New Benchmark Based on Recent Advances in Multispectral Pansharpening: Revisiting Pansharpening With Classical and Emerging Pansharpening Methods. IEEE Geosci Remote Sens Mag 9, 53–81. https://doi.org/ 10.1109/MGRS.2020.3019315.

Wald, L., Ranchin, T. and Mangolini, M., 1997: Fusion of satellite images of different spatial resolutions: Assessing the quality of resulting images. Photogrammetric engineering and remote sensing, 63(6), pp.691-699.

Wang, Y., Zhu, Q., Shi, Y., Song, M., Yu, C., 2021: A Spatial-Enhanced LSE-SFIM Algorithm for Hyperspectral and Multispectral Images Fusion. Remote Sens (Basel). https://doi.org/10.3390/rs13244967.

Yuhas, R.H., Goetz, A.F. and Boardman, J.W., 1992, June: Discrimination among semi-arid landscape endmembers using the spectral angle mapper (SAM) algorithm. In JPL, Summaries of the Third Annual JPL Airborne Geoscience Workshop. Volume 1: AVIRIS Workshop.

Zoran, L.F., 2009: Quality evaluation of multiresolution remote sensing images fusion. UPB Sci Bull Series C, 71(01).